Quantum Electronics **51** (3) 265–271 (2021) ©2021 Kvantovaya Elektronika and IOP Publishing Limited

https://doi.org/10.1070/QEL17507

Laser adaptive vector-phase hydroacoustic measuring system

R.V. Romashko, Yu.N. Kulchin, D.V. Storozhenko, M.N. Bezruk, V.P. Dzyuba

Abstract. **We have developed and experimentally implemented an adaptive laser vector-phase hydroacoustic measuring system, which allows one to determine the total acoustic intensity vector. A receiving element of the measuring system comprises six spatially separated fibre-optic coil-type sensors. Signals from the sensors are phase demodulated by using a six-channel adaptive holographic interferometer based on dynamic holograms multiplexed in a photorefractive CdTe crystal. Performance of the developed measuring system has been experimentally tested by determining the bearing and localisation of a source of a weak hydroacoustic field.**

Keywords: *fibre-optic sensor, adaptive interferometer, dynamic hologram, photorefractive crystal, hydrophone, vector-phase sensor, acoustic bearing.*

1. Introduction

Solving such problems as monitoring of sea and ocean areas, clarification of underwater environment, and some others requires the employment of high-sensitive sensors for detecting weak hydroacoustic signals [1–4]. Presently, hydroacoustic receivers based on electrical transducers (piezoelectric, electrodynamic, capacitive, etc.) are most widely used [5, 6]. However, such receivers have some drawbacks, which substantially limit the detection possibility in the case of weak hydroacoustic signals. Optical and fibre-optic sensors developed recently [7, 8] are an alternative to electrical hydrophones. Unlike conventional electrical sensors, fibre-optic sensors are insensitive to an electromagnetic background noise, withstand high temperatures, and can operate in corrosive media, which makes them promising in hydrophone development. In addition, the employment of interferometric detection principles in such sensors makes it possible to detect ultra-low signals due to the potentially high sensitivity of an optical interferometer [9–12]. In turn, the methods of adaptive interferometry based on two-wave mixing on the dynamic holograms recorded in a photorefractive crystal (PRC) [13–16] make it possible to exclude the internal instability of an optical interferometer [17] and to measure ultra-low physical parameters, such as nanoscale displacements, oscillations and vibrations, ultra-weak deformations, and others, against the background of external noise factors (random mechanical actions, industrial noise, temperature drift, etc.) [18–24]. Adaptive interferometry methods are also used for detecting weak acoustic signals in non-destructive testing [25–29], acoustic [30–33], seismic-acoustic [34, 35], and hydroacoustic [36–38] measurements. In these works, the scalar parameter of an acoustic field was measured, namely, an acoustic pressure. However, information about the value of the acoustic signal is not sufficient in many applications, in particular, in localising a source of an acoustic signal. In this case, one can successfully employ the vector-phase approach, which is based on an additional detection of the vibrational velocity of medium particles (or acoustic pressure gradient). This, in turn, makes it possible to determine the acoustic intensity vector, which carries information about the source position [39–41]. For determining the total gradient of an acoustic pressure, it is necessary to measure the acoustic pressure at three pairs of points arranged in three orthogonal directions at a certain separation from each other. This approach was used for creating a vector hydrophone in [42], where three fibre-optic Michelson interferometers were used for phase demodulation. Stabilisation and noise suppression in such a hydrophone consist in recording the certain phase signal induced by noise in the interferometer arms with its following subtraction from the interferometer output phase signal. For this purpose, an additional reference sensor isolated from external actions is included in the construction. In this case, the stability of the hydrophone output signal has been demonstrated for only a short time (2 min), and the long-term stability is not discussed. Basing on a two-channel adaptive interferometer, a laser adaptive hydroacoustic intensimeter was realised in [43], which detected one of three projections of an acoustic intensity vector to a chosen direction. Determination of the total acoustic intensity vector requires simultaneous measurement of the acoustic pressure at six points. Hence, an adaptive interferometer with at least six channels is necessary. It was experimentally shown [44] that a single PRC in the orthogonal geometry with two-wave mixing can provide formation of six and more dynamic holograms, the channels of the adaptive interferometer operating independently and the level of crosstalk not exceeding the interferometer intrinsic noise.

In the present work, we propose, experimentally realise and investigate a laser adaptive vector-phase hydroacoustic measuring system (VPAMS), in which the detector comprises six fibre-optic sensors of a coil type, and signals from the sen-

R.V. Romashko, Yu.N. Kulchin Institute of Automation and Control Processes, Far Eastern Branch of the Russian Academy of Sciences, ul. Radio 5, 690041 Vladivostok, Russia; Far Eastern Federal University, Ajax Bay 10, Russky Island, 690922 Vladivostok, Russia; e-mail: romashko@iacp.dvo.ru;
D.V. Storozhenko, M.N. Bezruk, V.P. Dzyuba Institute of Automation and Control Processes, Far Eastern Branch of the Russian Academy of Sciences, ul. Radio 5, 690041 Vladivastok, Russia

Received 14 December 2020
Kvantovaya Elektronika **51** (3) 265–271 (2021)
Translated by N.A. Raspopov

sors are demodulated by using a six-channel adaptive holographic interferometer based on dynamic holograms recorded in a single PRC. It was experimentally shown that the VPAMS provides determination of the total acoustic intensity vector. The VPAMS is tested for bearing and localising a source of a weak hydroacoustic field.

2. Acoustic intensity vector

A vector of an acoustic energy flux density $\boldsymbol{I}$ (the acoustic intensity vector) is defined in the frequency domain as the real part of the product of an acoustic pressure $p(\omega)$ and vibration velocity vector $\boldsymbol{V}(\omega)$ [39].

$$\boldsymbol{I}(\omega) = 0.5\mathrm{Re}(p(\omega)\boldsymbol{V}(\omega)), \quad (1)$$

where ω is the acoustic signal frequency. A vibration velocity vector is defined through the pressure gradient and medium density ρ:

$$\boldsymbol{V}(\omega) = -\frac{\nabla p(\omega)}{\mathrm{i}\rho\omega}. \quad (2)$$

In view of expressions (1) and (2), the components of vector $\boldsymbol{I}(\omega) = \{I_x, I_y, I_z\}$ at a space point $\boldsymbol{r}$ can be presented in the form:

$$I_j(\boldsymbol{r}) = -\frac{0.5p(\boldsymbol{r})}{\mathrm{i}\rho\omega}\frac{p(\boldsymbol{r}+\boldsymbol{d}_j/2) - p(\boldsymbol{r}-\boldsymbol{d}_j/2)}{d_j}, \quad j = x,y,z, \quad (3)$$

where $\boldsymbol{d}_j$ is the vector joining the two points in a vicinity of point $\boldsymbol{r}$, separated by distance d_j along axis j (Fig. 1a). Thus, for determining the vector $\boldsymbol{I}(\omega)$, it is necessary to find the acoustic pressure for three pairs of equidistant points disposed in three orthogonal axes. Here, the minimal length of the acoustic wave $\lambda_{\min}$ that can be detected in this way is determined by the maximal distance between pairs of the points, at which the acoustic pressure is measured: $\lambda_{\min} = 6d_0$, where $d_0 = \max\{d_x, d_y, d_z\}$.

3. Architecture of the laser adaptive VPAMS

A schematic of the the VPAMS receiving acoustic element, which provides primary recording of an acoustic signal, is shown in Fig. 1b. The receiving element comprises six fibre-optic sensors of the coil type. Each sensor is arranged on a cylinder fabricated from extrude polystyrene foam XPS with a diameter of 50 mm and a height of 20 mm. A multimode fibre (with a core diameter of 62.5 μm and a numeric aperture NA = 0.22) of length 5 m is wound onto the cylinder (30 winds).

As mentioned above, a measurement of three components of the pressure gradient requires pairwise sensors placed at the ends of the segments oriented along three mutually orthogonal spatial axes X, Y, Z (Fig. 1a). In order to meet this requirement, the VPAMS detection element was developed on the basis of a metal frame in the form of cuboctahedron (Figs 1b and 1c). The latter, in addition to triangle, has three pairs of square parallel faces arranged in such a way that the diagonals in each pair are oriented in three mutually orthogonal directions. In each diagonal, a single sensor (altogether six) is placed, which provides the fulfilment of the spatial requirements (Fig. 1a), the distance d_j between the sensors in each pair being the same and equal to 25 cm.

A schematic of a laser VPAMS is shown in Fig. 2. Radiation of a Nd : YAG laser (with a wavelength of 1064 nm, an output power of 1000 mW, anda coherence length of 300 m) passes through a half-wave phase plate, which rotates the polarisation plane in such a way that the radiation having passed through a polarisation beam splitter is split to a signal and reference light waves in the ratio 1:5. Then, the reference wave elliptically polarised after passing a quarter-wave plate is directed to a CdTe PRC of size 5×5×5 mm along the crystallographic axis [100]. In turn, the signal wave radiation is additionally split by a fibre-optic coupler 1×6 to six light waves directed to six fibre-optic sensors comprised in the VPAMS receiving element. Due to high radiation coherence, the distance between the detector element and adaptive interferometer may reach 100 m, which makes it possible to arrange the VPAMS receiving element at a substantial distance from the system itself. Mechanical vibrations of the sensor base material caused by an action of acoustic pressure lead to a phase modulation of the radiation of signal waves passing through the fibres. Then, the phase-modulated radiation from each sensor is directed through branching-off fibres to the PRC along the crystallographic axis [100] orthogonally to the reference wave. At the crystal input, the intensity of each signal wave was 1 mW mm^{-2}, and the reference wave intensity was 30 mW mm^{-2}. In a PRC with cubic symmetry, the vector interaction of the elliptically polarised reference wave with depolarised (after passing through multimode fibres) signal waves in this orthogonal geometry results in the recording of six dynamic holograms in the crystal. The diffraction of signal waves on these holograms provides a linear

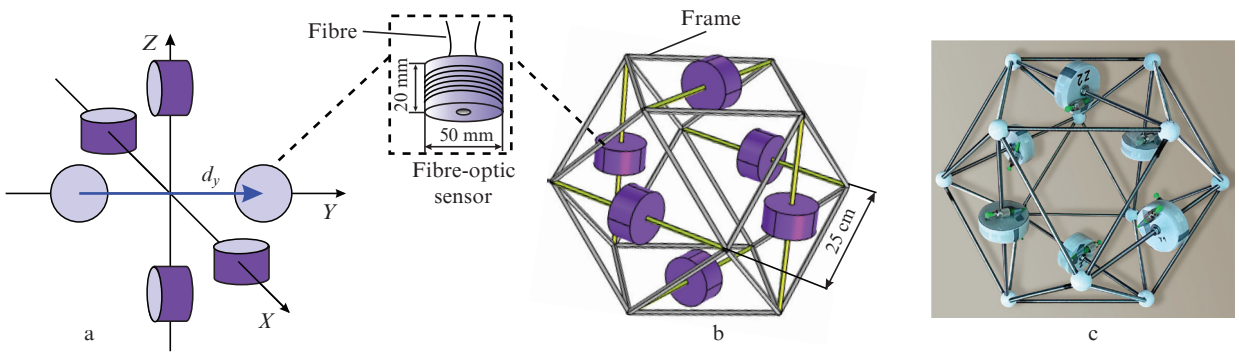

Figure 1. (a) Spatial arrangement geometry of the fibre-optic acoustic sensor for measuring an acoustic intensity (from vectors $\boldsymbol{d}_x$, $\boldsymbol{d}_y$ and $\boldsymbol{d}_z$, only the vector along Y axis is shown), as well as (b) schematic and (c) image of the receiving acoustic element of the laser adaptive VPAMS.

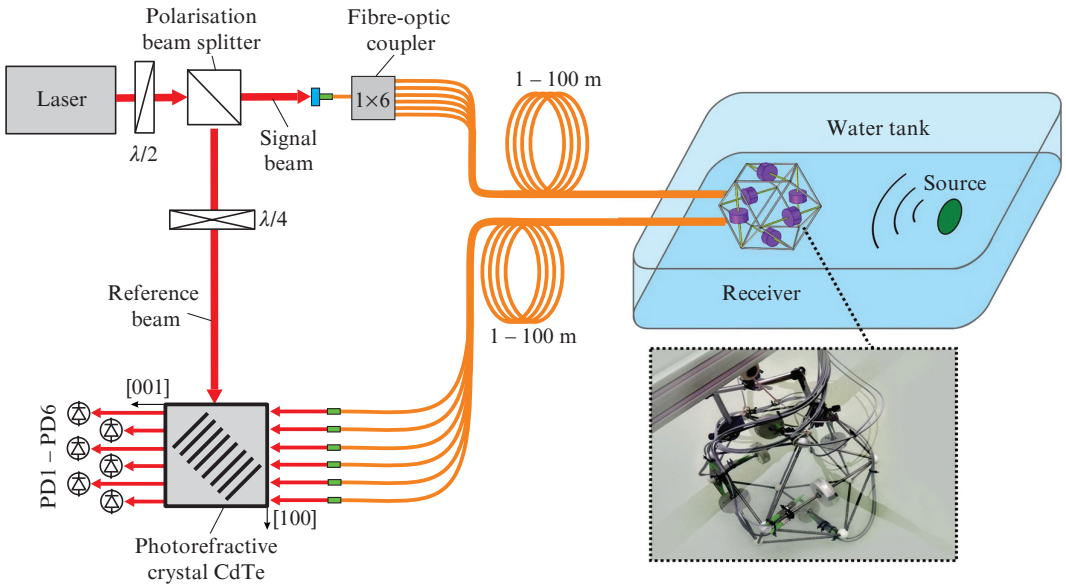

Figure 2. Schematic of an adaptive vector-phase acoustic measuring system. The inset shows an image of a receiving element of the measuring system in the water tank.

transformation of the phase modulation to intensity modulation [45, 46]. In view of the fact that the phase modulation of a light wave is proportional to the acoustic pressure, the electrical signals from photodetectors PD1–PD6 recording the radiation intensity in the six channels at the PRC output make it possible to determine the acoustic pressure at the positions of the six sensors.

The electric signals from each photodetector having passed through a zero-frequency-component filter are amplified by 30 dB and directed to a 12-bit ADC with the sampling frequency of 50 kHz. Then the digital signals are processed by using a software realised in MATLAB® package. According to this algorithm, the data obtained sequentially pass through a band filter adjusted to the frequency band of the expected signal and are subjected to the Fourier transform needed for obtaining the complex spectrum of the signal with the averaging period in the range of 0.1–4.0 s (depending on the experimental conditions). Basing on this complex spectrum and taking into account the system sensitivity determined preliminarily, the values of acoustic pressure at the points of fibre-optic sensor positions are calculated.

In order to find the intensity vector by using expression (3), in addition to measurements of acoustic pressure at six points in the directions X, Y, Z, it is necessary to determine pressure $p(\omega)$ at the geometrical centre of the VPAMS receiving element. In view of the fact that all the six sensors are equidistant from the centre of the VPAMS receiving element and a separation between elements is no longer than 1/6 of wavelength, the pressure $p(\omega)$ can be determined as an arithmetic mean of pressure values at positions of all sensors.

Note that, since determination of the vector of the acoustic pressure intensity is related to a variation of the acoustic pressure gradient, it is important for the sensitivities of all VPAMS channels to be the same. Sensitivity of a separate sensor is determined both by the sensitivity of a fibre-optic sensor (comprised in the receiving element) to acoustic pressure and by the phase sensitivity of an adaptive holographic interferometer. The sensitivity to acoustic pressure depends on the sensor shape, its geometrical dimensions, length of wound optical fibre, and may differ from sensor to sensor due to inevitable differences between actual and nominal parameters of the latter. The phase sensitivity of an adaptive interferometer in different channels may also differ for a number of reasons, such as photorefractive crystal inhomogeneity over volume (light beams in different channels fit to different PRC parts), different light wave amplitudes at the output from the fibre-optic coupler, and possible spread of photodetector characteristics.

In order to decrease such parameter variations, we used two-stage calibration of channel sensitivity in the adaptive interferometer suggested in [47] and developed in [48]. At the first calibration stage, the same phase modulation (calibration signal) with a linearly growing amplitude was introduced to all the interferometer channels. Then, the transient response was calculated and the calibration factors were determined for each channel. Such a calibration reduced the differences in the adaptive interferometer sensitivity to phase modulation. The differences in the fibre-optic sensor sensitivities to acoustic pressure were eliminated at the second calibration stage by placing each sensor in an acoustic field with known pressure (0.4 Pa); the signal processing was performed taking into account the calibration factors obtained at the first stage. Finally, after the total calibration cycle, the same sensitivities in VPAMS channels equal to 29 ± 0.12 V Pa^{-1} were provided.

4. Determining the acoustic source bearing

The possibility of the developed laser adaptive VPAMS to determine the direction to a hydroacoustic source from the measured acoustic intensity vector was studied experimentally in the laboratory conditions, which simulated an open underwater medium. For this purpose, a test water tank was used with the dimensions of $2.6 \times 1.7 \times 0.6$ m filled to 80% with fresh water; the water tank was arranged on a sand substrate. Measurements were taken at a water temperature of 10 °C, the sound velocity in water was 1450 m s^{-1} [49]. The acoustic source was an electrodynamic projector with the radiation pattern presented in Fig. 3. The source was plunged in water to a depth of 25 cm from bottom, which coincided with the VPAMS receiving element depth.

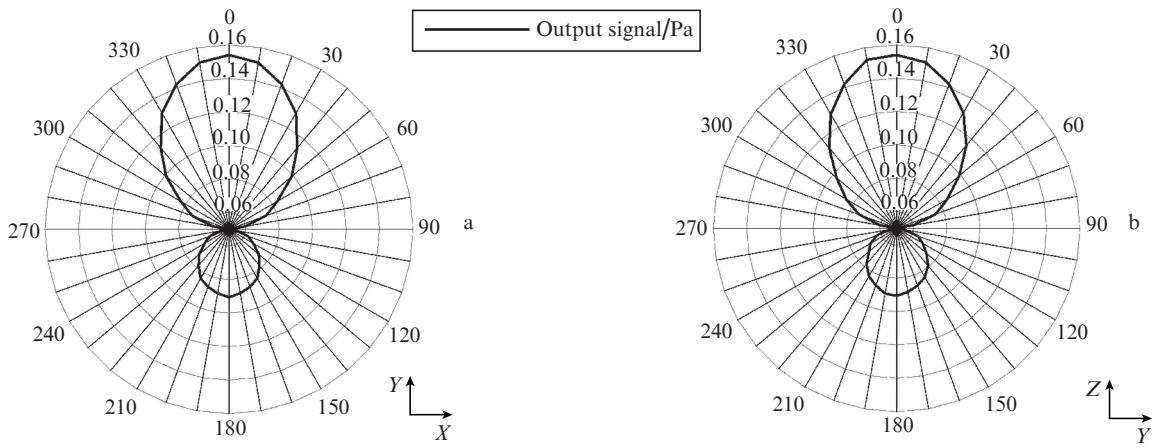

Figure 3. Angular direction characteristics of the electrodynamic hydroacoustic projector operated at a frequency of 900 Hz in planes (a) *XY* and (b) *YZ*.

Since the VPAMS was tested in a water tank of limited dimensions, and reflections from its walls might arise, it was necessary to provide the conditions in which these reflections may be neglected and one might assume that the bearing of the signal source is the reverse of the intensity vector. With this purpose, the acoustic field produced in a limited water tank was simulated by using the COMSOL Multiphysics® software package with the Acoustic Toolbox module. A phys-

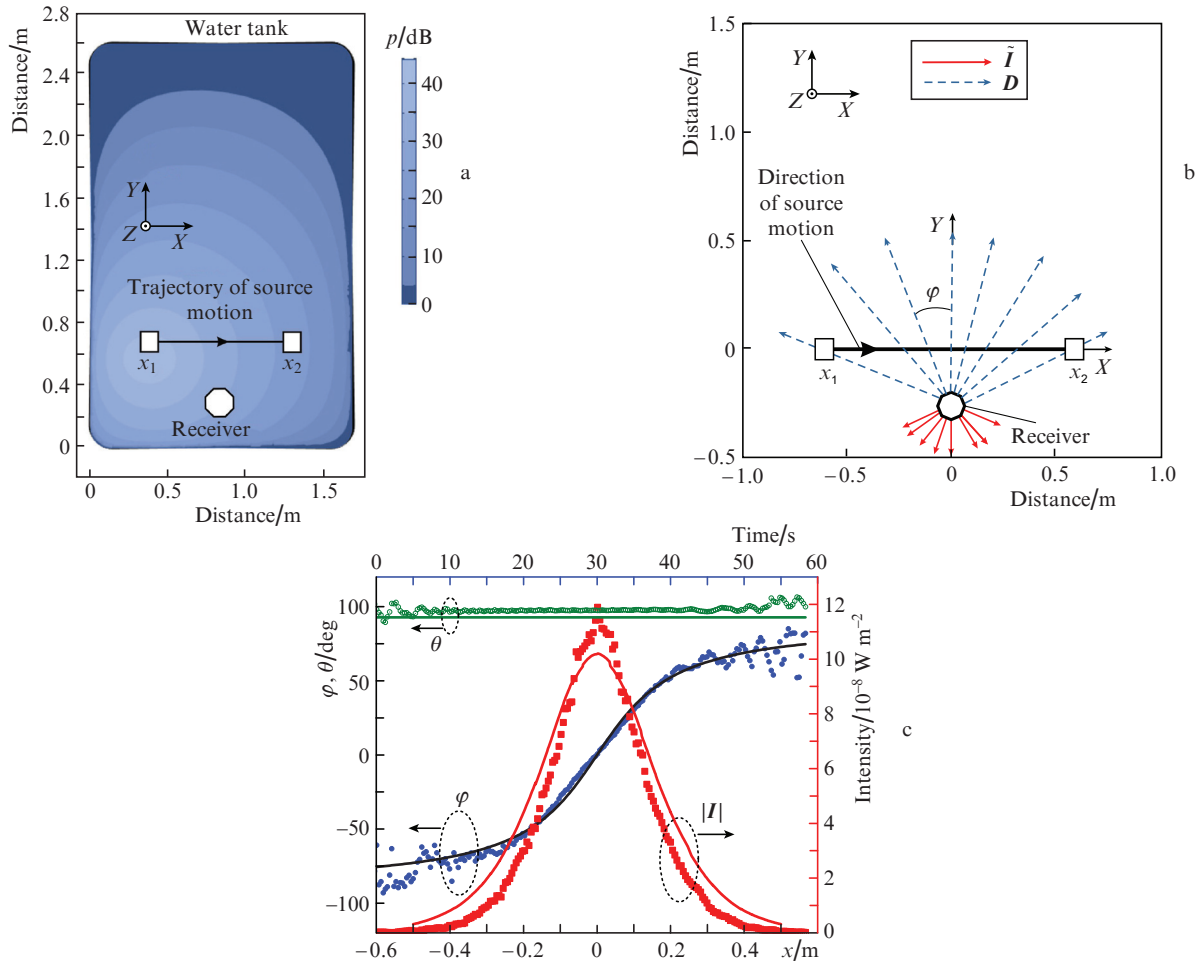

Figure 4. Scheme and results of the experimental study of VPAMS operation for bearing on a moving acoustic source: (a) amplitude distribution of a model acoustic field in a test water tank at a frequency of 900 Hz and scheme of acoustic source motion relative to the VPAMS receiver; (b) experimentally obtained unit vectors for acoustic intensity $\tilde{\boldsymbol{I}}$ and vectors $\boldsymbol{D}$ for hydroacoustic source bearing (the scales are not mutually matched); (c) diagram of the intensity vector modulus $|\boldsymbol{I}|$ and the azimuth (φ) and zenith (θ) angles, which determine the vector of the bearing on a moving hydroacoustic source (dots correspond to experimental data, solid curves refer to calculated dependences).

ical interface of this model is a solution of Helmholtz equation by the finite-element method in the frequency domain with a perfectly matched layer at the boundary of the calculation domain which the geometrical volume was 11 m^3. The mesh of the tetrahedron type had the number of elements 1.1×10^6. The model uses the assigned radiation pattern of the hydroacoustic source, density and acoustic speed for fresh water (ρ = 1000 kg m^{-3}, c = 1450 m s^{-1}) filling the water tank, for soil (ρ = 1800 kg m^{-3}, c = 1600 m s^{-1}), and for ambient air (ρ = 1.2 kg m^{-3}, c = 343 m s^{-1}). Geometry of the calculation domain allowed for the dimensions (2.6×1.7×0.48 m) and specific shape features of a real water tank [43]. From the model calculation, it was found that in the frequency range of 100 – 1500 Hz, reflections from water boundaries (water tank walls) do not significantly affect the acoustic field distribution, which is illustrated in Figs 4a and 5a. Thus, the working frequency of 900 Hz was chosen for acoustic source tests; the wavelength in water at this frequency is λ = 1.6 m ($\lambda > \lambda_{min} = 6d_0$ = 1.5 m).

In the experiment, the acoustic source evenly and rectilinearly moved at a speed of 2 cm s^{-1} in the water tank along the X axis from point x_1 to point x_2 separated by a distance of 1 m by using a motorised translator (Fig. 4a). The VPAMS receiving element was 25 cm apart from the line of source motion. The VPAMS output signal was recorded instantaneously for the total time of the source motion (60 s). From the signal obtained, periods of duration 0.3 s were sequentially chosen for calculating the pressures at six points of sensor positions. Then, the vector of the acoustic intensity $\boldsymbol{I}$ was calculated by expression (3); thus, the source position was determined at 207 points, which corresponds to a source motion step of approximately 5 mm. Unit intensity vectors obtained in this way $\tilde{\boldsymbol{I}} = \boldsymbol{I}/|\boldsymbol{I}|$ and the reverse vectors corresponding to the source bearing $\boldsymbol{D} = -\tilde{\boldsymbol{I}}$ are shown in Fig. 4b. For clearness, vectors $\tilde{\boldsymbol{I}}$ and $\boldsymbol{D}$ are shown separately for certain source positions. In Fig. 4c, one can see the calculated and VPAMS experimental diagrams for azimuthal φ (the angle between vector $\boldsymbol{D}$ and Y axis) and zenith θ (the angle between vector $\boldsymbol{D}$ and Z axis) angles along with the absolute value of the intensity vector $|\boldsymbol{I}|$. In the diagram, the measured dependences φ and θ were plotted by using the time readings (basing on the components of vector $\boldsymbol{I}$, obtained with VPAMS at instant t), and the calculated dependences were plotted according to an *a priori* known source geometrical position on the X axis at measurement instant t. One can see from Fig. 4c that, despite of a certain discrepancy in values of $|\boldsymbol{I}|$, the calculated and measured values of angle φ to a sufficiently high accuracy coincide in the range φ = [–55°, 55°], with the angle rms deviation (RMSD) of 3.3°. At greater bearing angles (more than ±55°), the deviation increased to 10.4°, which is explained by worsening the signal/noise (S/N) ratio due to the reduction of signal amplitude, caused by recession

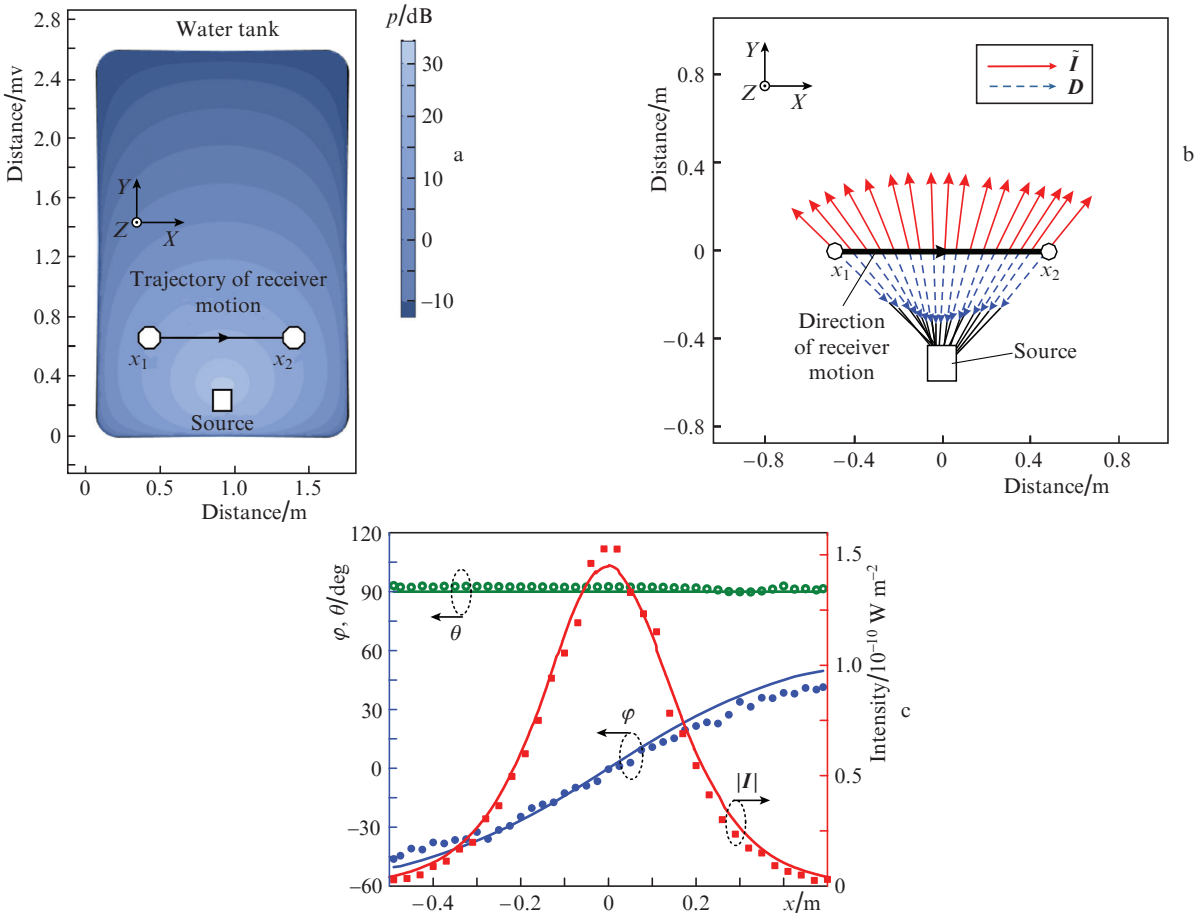

Figure 5. Scheme and results of VPAMS experimental study on localising a stationary acoustic source by using a moving receiver: (a) amplitude distribution of a model acoustic field in the test water tank with fixed source and trajectory of receiver motion; (b) measured unit vectors of intensity $\tilde{\boldsymbol{I}}$ and vectors $\boldsymbol{D}$ of hydroacoustic source bearing; (c) diagram of the intensity vector modulus $|\boldsymbol{I}|$, and azimuth (φ) and zenith (θ) angles (dots correspond to experimental data, solid lines refer to calculated dependences).

of the source, which has a high anisotropy of directional pattern, from the receiver. Since, in the framework of the experiment geometry, the source and receiver all the time kept the same depth, the expected value of zenith angle θ was 90°. In Fig. 4c, the dependence $\theta(x)$ obtained with the VPAMS is presented, from which follows that, in the case of a sound source fitting the range x = [–0.4 m, 0.4 m] (in which the required detected S/N ratio is provided) the experimental value of zenith angle θ is actually constant and equals to 98° ± 1°. The deviation of the measured θ from calculated value (expected 90°) to higher values, seemingly, is related to the acoustic wave reflection from the water tank bottom. Note that errors of determining angles φ and θ in the case of employing the VPAMS at a low S/N ratio can be reduced by making the signal averaging time longer.

5. Determining the acoustic source position

We also studied the VPAMS experimentally for determining a position of an acoustic source. Note that this requires either the employment of several receivers, or performing measurements with a single receiver at several points in space. With this purpose, the VPAMS receiving element moved to a distance of 1 m with a step of 2.5 cm along the X axis from point x_1 to point x_2 relative to the immovable acoustic source placed at the point with the coordinates $x = 0$, $y = -0.4$ m (Figs 5a and 5b). At each step, the receiver stopped and measured the acoustic signal for 2 s. Unit intensity vectors $\tilde{\boldsymbol{I}}$ and the corresponding reverse source bearing vectors $\boldsymbol{D}$ obtained in these measurements are presented in Fig. 5b. Here, the coordinates of the initial point for each vector $\tilde{\boldsymbol{I}}$ employed the receiver position at the instant of measurement.

The diagrams of calculated and measured angles φ and θ presented in Fig. 5c along with the diagram of the absolute value of intensity vector $|\boldsymbol{I}|$ well coincide. Here, RMSD for measured angles φ in the range [–35°, 35°] does not exceed 6°. An increase of RMSD to 9° at bearing angles of more than ±35° is related to the reduction in the S/N ratio due to receiver departure from the source, because the latter has a substantial anisotropy. From Fig. 5b one can see that the greater part of $\boldsymbol{D}$ vectors converge in the domain, where the source was arranged, which demonstrates successful determination of the source position by the receiving system. By using data obtained with the VPAMS, we also determined the zenith angle θ (Fig. 5c). Under the receiver motion in the whole range of its positions, the experimental value of angle theta actually did not change and was 95.5 ± 1.6°. Here, similarly to the previous case (see Fig. 4), a constant deviation of angle θ from calculated values is observed, which, seemingly, is related to the reflection of a sound wave from the water tank bottom.

6. Conclusions

Thus, in the present work we suggested, created, and studied a new type of a laser adaptive vector-phase hydroacoustic measuring system based on the six-channel adaptive holographic interferometer with the employment of dynamic holograms recorded in a single photorefractive crystal. The VPAMS also includes the fiber-optical sensors of acoustic signals, which are spatially arranged in such a way that three components of the acoustic pressure gradient can be recorded. It is shown that data recorded with the developed VPAMS allow one to obtain the total acoustic intensity vector. Using the developed VPAMS, we have demonstrated the possibility of determining the real-time bearing of a moving object with an accuracy of up to 3.3° and the possibility of determining a position of a weak hydroacoustic field. The employment of measuring systems of this type opens new possibilities in solving problems concerning determination of energy, interphase, coherent, and probabilistic properties of weak acoustic fields. This, in turn, may become a basis for developing new efficient revealing algorithms and methods of determining the bearing of weak acoustic sources and for development approaches to classifying such sources.

Acknowledgements. The work was supported by the Russian Scientific Foundation (Grant No. 19-12-00323).

References

1. Howe B.M., Miksis-Olds J., Rehm E., Sagen H., Worcester P.F., Haralabus G. *Front. Marine Sci.*, **6**, 426 (2019).
2. Venkatesan R., Tandon A., D'Asaro E., Atmanand M.A. *Observing the Oceans in Real Time* (Springer International Publishing, 2018).
3. Morgunov Yu.N. Doct. Thesis (POI FEB RAS, Vladivostok, 2001).
4. Laverov N.P., Popovich V.V., Vedeshin L.A., Konovalov V.E. *Sovr. Probl. DZZ Kosm.*, **14** (3), 141 (2017).
5. Sverdlin G.M. *Prikladnaya gidroakustika* (Applied Hydroacoustics) (Leningrad: Sudostroenie, 1990).
6. Bjørnø L. *Applied Underwater Acoustics* (Amsterdam: Elsevier, 2017).
7. Busurin V.I., Nosov Yu.R. *Volokonno-opticheskie datchiki* (Fibre-Optic Sensors) (Moscow: Energoatomizdat, 1990).
8. Udd E. *Fiber Optic Smart Structures* (New York: John Wiley & Sons Inc., 1995).
9. Wagner J.W., Spicer J. *J. Opt. Soc. Am. B*, **4**, 1316 (1987).
10. Abbott B.P. et al. *Phys. Rev. Lett*., **116** (6), 061102 (2016).
11. Beverini N., Basti A., Bosi F., Carelli G., Ciampini D., Di Virgio A., Ferrante I., Fuso F., Giacomelli U., Maccioni E., Simonelli A., Stefani F., Terreni G., Altucci C., Portzio A., Velotta R. *Quantum Electron*., **49** (2), 195 (2019) [*Kvantovaya Elektron*., **49** (2), 195 (2019)].
12. Gordeev A.A., Efimkov V.F., Zubarev I.G., Mikhailov S.I. *Quantum Electron*., **49** (9), 878 (2019) [*Kvantovaya Elektron.*, **49** (9), 878 (2019)].
13. Kamshilin A.A., Petrov M.P. *Opt. Commun*., **53**, 23 (1985).
14. Stepanov S.I., in *International Trends in Optics* (New York: Academic, 1991) Ch. 9.
15. Petrov M.P., Stepanov S.I., Khomenko A.V. *Photorefraktivnye kristally v kogerentnoi optike* (Photorefractive Crystals in Coherent Optics) (Saint-Petersburg: Nauka, 1992).
16. Shandarov S.M., Burimov N.I., Kul'chin Yu.N. *Quantum Electron*., **38** (11), 1059 (2008) [*Kvantovaya Elektron*., **38** (11), 1059 (2008)].
17. Krylov G.M., Fat'yanov O.V., Duplinskii A.V. *Quantum Electron*., **50** (5), 447 (2020) [*Kvantovaya Elektron*., **50** (5), 447 (2020)].
18. Kamshilin A.A., Romashko R.V., Kulchin Y.N. *J. Appl.Phys*., **105**, 031101 (2009).
19. Romashko R.V., Kulchin Y.N., Girolamo S.D., Kamshilin A.A., Launay J.C. *Key Eng. Mater*., **381–382**, 61 (2008).
20. Romashko R.V., Efimov T.A., Kulchin Yu.N. *Quantum Electron*., **44** (3), 269 (2014) [*Kvantovaya Elektron*., **44** (3), 269 (2014)].
21. Romashko R., Efimov T., Kulchin Y. *J. Russ. Laser Res*., **37** (1), 102 (2016).
22. Stepanov S., Casillas D.G., Cota F.P., Hernández E.H., Sánchez M.P., Montero P.R., in *CLEO/Europe and IQEC 2007 Conference Digest* (USA: Opt. Soc. Am., 2007) paper CC3_3.
23. Di Girolamo S., Kamshilin A.A., Romashko R.V., Kulchin Y.N., Launay J.C. *Opt. Lett*., **32** (13), 1821 (2007).
24. Bryushinin M.A., Kulikov V.V., Petrov A.A., Sokolov I.A., Romashko R.V., Kulchin Y.N. *Appl. Opt*., **59** (8), 2370 (2020).
25. Ja Y.H. *Opt. Laser Technol.*, **17** (1), 36 (1985).

26. Murray Todd W., Tuovinen H., Krishnaswamy S. *Appl. Opt.*, **39**, 3276 (2000).
27. Berer T., Hochreiner A., Zamiri S., Burgholzer P. *Opt. Lett*., **35**, 4151 (2010).
28. Bashkov O.V., Romashko R.V., Zaikov V.I., Panin S.V., Bezruk M.N., Khun K., Bashkov I.O. *Russ. J. Nondestruct. Testing*, **53** (6), 415 (2017).
29. Jacquot P., Fournier J.M. (Eds) *Interferometry in Speckle Light* (Berlin: Springer Intern. Publ., 2000) pp 171–178.
30. Romashko R.V., Kulchin Y.N., Nippolainen E. *Laser Phys*., **24** (11), 115604 (2014).
31. Romashko R.V., Efimov T.A., Kulchin Y.N. *Proc. SPIE*, **10176**, 1017616 (2016).
32. Bryushinin M.A., Kulikov V.V., Mokhov E.N., Romashko R.V., Sokolov I.A. *Optik*, **127** (1), 341 (2016).
33. Romashko R.V., Bezruk M.N., Ermolaev S.A., Storozhenko D.A., Kulchin Y.N. *Proc. SPIE*, **10176**, 1017612 (2016).
34. Kamenev O.T., Petrov Yu.S., Khizhnyak R.V., Zavestovskaya I.N., Kulchin Yu.N., Romashko R.V. *Bull. Lebedev Phys. Inst*., **44** (7), 202 (2017) [*Kr. Soobshch. Fiz. FIAN*, **44** (7), 27 (2017)].
35. Kamenev O.T., Romashko R.V., Kulchin Yu.N. *Lazernye priemniki seismo- i gydroakusticheskikh signalov* (Laser Detectors for Seismic and Hydro-Acoustic Signals) (Novosibirsk: Izd. SB RAS, 2016).
36. Romashko R.V., Bezruk M.N., Ermolaev S.A., Zavestovskaya I.N., Kulchin Yu.N. *Bull. Lebedev Phys. Inst.*, **42** (7), 201 (2015) [*Kr. Soobshch. Fiz. FIAN*, **42** (7) 14 (2015)].
37. Romashko R.V., Kulchin Yu.N., Bezruk M.N., Ermolaev S.A. *Quantum Electron*., **46** (3), 277 (2016) [*Kvantovaya Elektron*., **46** (3), 277 (2016)].
38. Kulchin Yu.N., Voznesenskii S.S., Gamayunov E.L., Golik S.S., Il'in A.A., Kamenev O.T., Nikitin A.I., Pavlov A.N. *Quantum Electron*., **50** (5), 475 (2020) [*Kvantovaya Elektron*., **50** (5), 475 (2020)].
39. Gordienko V.A. *Vektorno-fazovye metody v akustike* (Vector-Phase Methods in Acoustics) (Moscow: Fizmatlit, 2007).
40. Gordienko V.A., Gordienko T.V., Krasnopistsev N.V., Nekrasov V.N. *Moscow Univ. Phys. Bull*., **69** (2), 105 (2014) [*Vestnik Mosk. Universiteta, Ser. 3. Fiz. Astron*., (2), 3 (2014)].
41. Dzyuba V.P. *Skalyarno-vektornye metody teoreticheskoi akustiki* (Scalar-Vector Methods in Theoretical Acoustic) (Vladivostok: Dal'nauka, 2006)].
42. Wang J., Luo H., Meng Z., Hu Y. *J. Lightwave Technol*., **30** (8), 1178 (2011).
43. Romashko R.V., Kulchin Yu.N., Dsyuba V.P., Storozhenko D.V., Bezruk M.N. *Quantum Electron*., **50** (5), 514 (2020) [*Kvantovaya Elektron*., **50** (5), 514 (2020)].
44. Romashko R.V., Bezruk M.N., Kamshilin A.A., Kulchin Yu.N. *Quantum Electron*., **42** (6), 551 (2012) [*Kvantovaya Elektron*., **42** (6), 551 (2012)].
45. Di Girolamo S., Kamshilin A.A., Romashko R.V., Kulchin Yu.N., Launay J.-C. *Opt. Express*, **15** (2), 545 (2007).
46. Romashko R.V., Di Girolamo S., Kulchin Y.N., Kamshilin A.A. *J. Opt. Soc. Am. B*, **27** (2), 311 (2010).
47. Romashko R.V., Bezruk M.N., Ermolaev S.A., Zavestovskaya I.N. *Bull. Lebedev Phys. Inst*., **41**, 348 (2014) [*Kr. Soobshch. Fiz.. FIAN*, **41** (12), 8 (2014)].
48. Bezruk M.N., Romashko R.V., Kulchin Yu.N., Ermolaev S.A., Notkin B.S. *Vestnik FEB RAS*, (2), 117 (2019) [*Vestnik DVO RAS*, (2), 117 (2019)].
49. Belogolskii V.A., Sekoyan S.S., Samorukova L.M., Stefanov S.R., Levtsov V.I. *Measur. Techniq*., **42**, 406 (1999) [*Izm. Tekh*., (4), 66 (1999)].